Composite CaO-Based CO$_2$ Sorbents Synthesized by Ultrasonic Spray Pyrolysis: Experimental Results and Modeling

Maryam Sayyah,[†] Emadoddin Abbasi,[‡] Yongqi Lu,[§] Javad Abbasian,[‡] and Kenneth S. Suslick*,[†]

[†]School of Chemical Sciences, University of Illinois at Urbana−Champaign, 600 S. Mathews Ave., Urbana, Illinois 61801, United States

[‡]Department of Chemical and Biological Engineering, Illinois Institute of Technology, Chicago, Illinois 60616, United States

[§]Illinois State Geological Survey, Prairie Research Institute, University of Illinois at Urbana−Champaign, 615 E. Peabody Dr., Champaign, Illinois 61820, United States

S *Supporting Information*

ABSTRACT: We report the preparation of calcium oxide (CaO)-based sorbents by ultrasonic spray pyrolysis (USP) with both experimental results and modeling of the sorption process. To mitigate CaO deactivation during carbonation/regeneration cycles, metal oxides with high melting temperatures were dispersed into CaO particles in this bottom-up synthetic method (USP), and their performance was experimentally characterized and evaluated over 50 cycles. The performance of synthesized sorbents was then compared to those expected from an unreacted shrinking core model. The model was able to predict the experimental results and provide an explanation for the effect of sintering and agglomeration on the performance of the sorbents through a variable effective diffusivity. Moreover, it was used to extrapolate sorbent performance over large numbers of cycles.

1. INTRODUCTION

Developing new CO$_2$ capture processes and materials is an active area of research focused on finding more cost-effective ways to implement carbon capture and storage (CCS) from large-point sources such as power plants. Of particular interest, precombustion CO$_2$ capture (from coal synthesis gases produced in gasification-based processes) has the advantages of high CO$_2$ concentrations and elevated operating pressures, which reduces the energy penalty associated with carbon capture to 10%−16% (i.e., roughly half of that for postcombustion CO$_2$ capture).[1] Among emerging precombustion processes, sorption-enhanced water−gas shift (SEWGS) reaction process, which combines the WGS reaction and CO$_2$ removal into a single process step in an integrated gasification combined cycle (IGCC) power plant, has attracted a growing interest. The SEWGS approach shifts the equilibrium of the exothermic WGS reaction (CO + H$_2$O ↔ CO$_2$ + H$_2$) toward H$_2$ by removing CO$_2$ as it is formed. This enables higher temperature WGS operation, which has benefits of reduced parasitic power losses from cooling and reheating the gas stream, reduced or even eliminated need for a WGS catalyst, and a reduced number of unit operations.[2,3]

To be applicable for SEWGS processes, regenerable CO$_2$ selective sorbents with decent CO$_2$ sorbing capacity, fast kinetics, and high thermal/mechanical stability are required. Among high-temperature CO$_2$ sorbents, calcium oxide (CaO) is a particularly attractive choice, because of its relatively low cost, high capacity, fast kinetics, and selectivity. CaO, however, suffers from performance degradation after multiple carbonation/regeneration cycles, mainly because of sintering,[1] a reduction of surface area,[4,5] and a loss of microporosity.[6,7] This issue must be mitigated before CaO can be of practical use. Among many of such efforts, the addition of supports and binders such as refractory metal oxides has been proposed as the most beneficial approach to improve the performance and reversibility of CaO.[8]

Aerosol synthesis methods have been extensively utilized to prepare a variety of metal oxides, even on an industrial scale.[9,10] Recently, we reported the first use of ultrasonic spray pyrolysis (USP) to prepare Al$_2$O$_3$−CaO composite sorbents for CO$_2$ capture.[11] In this work, we extend the use of USP for the synthesis of a variety of composite CaO-based materials. Unlike many batch synthesis methods examined in the literature,[12−15] USP provides a continuous flow approach for the facile preparation of CaO-based materials; given the amounts of sorbents needed for any practical use of CO$_2$ capture, any useful synthetic method must be a flow process, not a batch process. USP synthesis had the additional advantages of uniform distribution of additive species in CaO particles and improved yield of smaller particles, both of which contributed to an enhanced sorbent performance.[11] To improve cyclic reversibility of the prepared sorbents, several refractory metal oxides with high melting temperatures[16] such as Al$_2$O$_3$, MgO, SiO$_2$, and Y$_2$O$_3$ were dispersed into CaO particles in a bottom-up approach, and their performance over 50 cycles of carbonation/regeneration were experimentally compared. A variable diffusivity shrinking core model was then utilized to model the performance of the sorbents and to obtain quantitative parameters of interest for equipment design including effective diffusivity and its decay rate. The objective of the current study is thus to examine the efficacy of the metal oxide additives to mitigate CaO sintering and to develop a simplified approach to quantify the materials' degradation performance via a shrinking core model.

2. EXPERIMENTAL SECTION

To synthesize the composite CaO-based materials, an ethanol solution of calcium nitrate tetrahydrate [$Ca(NO_3)_2 \cdot 4H_2O$] and the respective additive oxide precursors (listed in Table 1) were nebulized via

Table 1. Additive Metal Oxides and Their Respective Precursors

additive	melting point[a] (°C)	precursor
MgO	2852	$Mg(NO_3)_2 \cdot 6H_2O$
Y_2O_3	2425	$Y(NO_3)_3 \cdot 6H_2O$
Al_2O_3	2050	$Al(NO_3)_3 \cdot 9H_2O$
SiO_2	1600	TEOS (tetraethyl orthosilicate)

[a]Data taken from ref 16.

ultrasound (2 MHz), and the resulting mist was carried through a furnace tube by argon gas. In the case of SiO_2 addition, 20 vol % water was added to ethanol to help hydrolysis of tetraethyl orthosilicate (TEOS). All chemicals were from Aldrich, >99% purity grade, and used as received. The total precursor concentration was kept at 0.25 M. CaO-based sorbents were synthesized with a 20:80 wt % additive oxides to CaO content ratio, and the USP furnace temperature was set at 600 °C. Solvent evaporation and precursor decomposition occurred within the furnace, and the product was collected in a laboratory-scale electrostatic precipitator (ESP). A schematic of the USP setup and the formation of composite particles via USP are presented in the Supporting Information (SI) (Figures S1 and S2, respectively) .

The four additive oxide precursors were selected in this study, either because of their relatively low prices for practical application (Mg, Al and Si) or for comparison purposes (Y). It has been previously noted that Al_2O_3 forms calcium aluminate phases upon reaction with CaO at high temperatures (e.g., $Ca_{12}Al_{14}O_{33}$, $Ca_3Al_2O_6$, $CaAl_2O_4$);[12] Ca_2SiO_4 and $CaSiO_3$ are also reported, in the case of SiO_2 addition.[17,18] In order to compare the performance of composite CaO-based sorbents in this work, all the sorbents' composition is based on 80 wt % *free* CaO content after the respective mixed oxide phases were formed. Therefore, the compositions are based on nominal 80:20 wt % $CaO:Ca_{12}Al_{14}O_{33}$, $CaO:Ca_2SiO_4$, $CaO:Y_2O_3$, $CaO:MgO$. In the case of combined alumina and silica addition, the composition is based on 80:10:10 wt % $CaO:Ca_{12}Al_{14}O_{33}:Ca_2SiO_4$.

The CO_2 capture performance of the synthesized sorbents was examined using a ThermoScientific VersaTherm thermogravimetric analyzer (TGA). Approximately 20 mg of sample was loaded into a quartz sample boat; carbonation and calcination cycles were performed at 700 °C for 30 min under 100% CO_2 and 950 °C for 5 min under 100% N_2, respectively. The flow rates of CO_2 and N_2 were kept at 35 sccm for all experiments. In practical application, increasing the adsorption temperature reduces the cooling and reheating requirement and also increases the reaction rate of CO_2 sorption, which results in higher CO_2 uptake over a finite reaction time (e.g., 30 min). However, the carbonation reaction is exothermic and the CO_2 adsorption equilibrium is adversely impacted with increasing temperature. Therefore, 700 °C was chosen as the optimum carbonation temperature throughout this work. The regeneration temperature was varied in a range of 900−1100 °C. Increasing desorption temperature beyond 950 °C worsened the sorbent's performance (see Figure S3 in the Supporting Information) due to aggravated sintering at high temperature.[12] Thus, 950 °C was chosen as the optimum regeneration (calcination) temperature throughout this work. N_2 is used for CO_2 desorption in the TGA tests to simulate a steam carrier gas in practice.

A typical syngas entering a water gas shift reactor contains ~10% CO_2, ~20% CO, ~20% H_2, and ~50% H_2O at 30−40 bar, depending on gasification technologies.[19] CO_2 concentration in the SEGWS process comes from two sources: CO_2 from the syngas, as well as CO_2 product from CO conversion in the water gas shift reaction. This corresponds to a CO_2 partial pressure of ~0.9−1.2 bar in the residue gas after the water gas shift reaction. The emphasis of this study was on investigations into the CO_2 adsorption performance of the USP sorbents. Therefore, 100% CO_2 gas at 1 bar was used in this work in order to provide the same partial pressure of CO_2, relevant to SEWGS.

3. RESULTS AND DISCUSSION

The sorbents were studied over 50 cycles of carbonation/ regeneration and compared to the pure USP-made CaO, as shown in Figure 1. Overall, the incorporation of inert metal
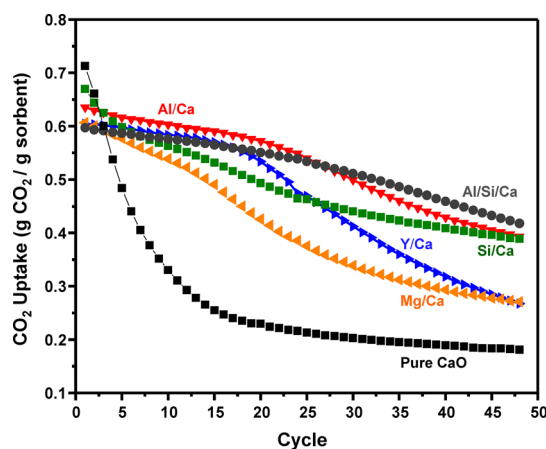

Figure 1. CO_2 capture performance during 50 cycles of carbonation/ regeneration for composite CaO sorbents compared with pure CaO sorbent. The cycling conditions were carbonation at 700 °C for 30 min under 100% CO_2 and regeneration at 950 °C for 5 min under 100% N_2. Al, Si, and Al/Si containing sorbents show the greatest improvement in the sorbent stability in extended operating cycles.

oxide binders shows a substantial enhancement in the CaO cycling stability. Al and Si proved to be the most effective additives to maintain high CaO capacity, while Mg and Y did not prove to work as effective in the long run, even though they possess the highest melting temperatures among the additives tested. This suggests that melting temperature alone cannot be the only factor causing the improved performance of composite CaO-based sorbents in this study. A composite Si/Al/Ca sorbent with nominal 80:10:10 wt % $CaO:Ca_{12}Al_{14}O_{33}:Ca_2SiO_4$ was also studied in the same fashion, and it retained the highest CO_2 capacity at cycle 50 among all the materials tested.

Composite CaO-based sorbents were further characterized using SEM, XRD, and BET surface area analysis. A three-point BET surface area analysis was used to measure the surface area of sorbents, as synthesized. The surface areas of all the sorbents were in the range of 5−18 m^2 g^{-1}. The SEM images below (Figures 2 and 3) show the changes in the morphology of alumina- and yittria-containing samples in the course of 50 cycles. As synthesized, the sorbents were nonagglomerated microparticles; however, as the materials underwent carbonation/regeneration cycling, the particles agglomerated. In Figures 2b and 3b, after 15 cycles, a roughly spherical particle morphology (with larger sizes) is still observed. After 50 cycles, severe sintering is evident in Figures 2c and 3c.

The composite CaO-based samples were also characterized by XRD. The XRD patterns of the as-synthesized sorbents in most cases showed only crystalline $CaCO_3$. In the case of yittria composites, $Ca(OH)_2$ was also observed, along with $CaCO_3$. As the materials were cycled, peaks corresponding to additive oxide phases appeared. Low content of additives makes the phase assignment of mixed oxides challenging. This is especially true for silicon- and aluminum-containing samples where mixed
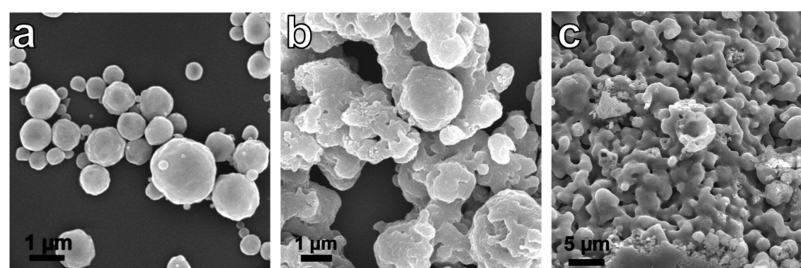
Figure 2. SEM of the composite sample with 80:20 wt % CaO:$Ca_{12}Al_{14}O_{33}$ (a) as-synthesized, (b) after 15 cycles, and (c) after 50 cycles. Severe particle agglomeration is evident with an increased number of carbonation/regeneration cycles.
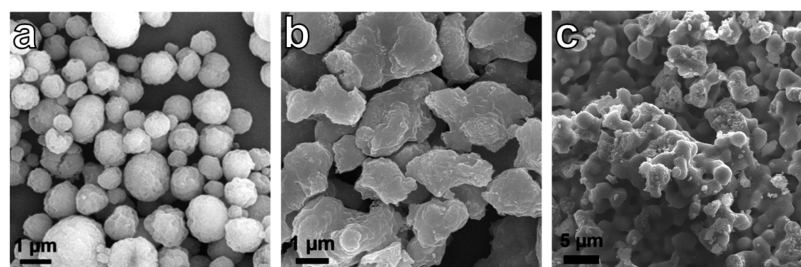

Figure 3. SEM of the sample with 80:20 wt % CaO:Y_2O_3 (a) as-synthesized, (b) after 15 cycles, and (c) after 50 cycles. Severe particle agglomeration is evident with an increased number of cycles.

oxide phases have been reported to be formed.[12,20] For example, for the aluminum-containing sorbent, many characteristic peaks of $Ca_3Al_2O_6$ and $Ca_{12}Al_{14}O_{33}$ phases overlap. Figures 4 and 5 show the XRD patterns of the samples with 80:20 wt %
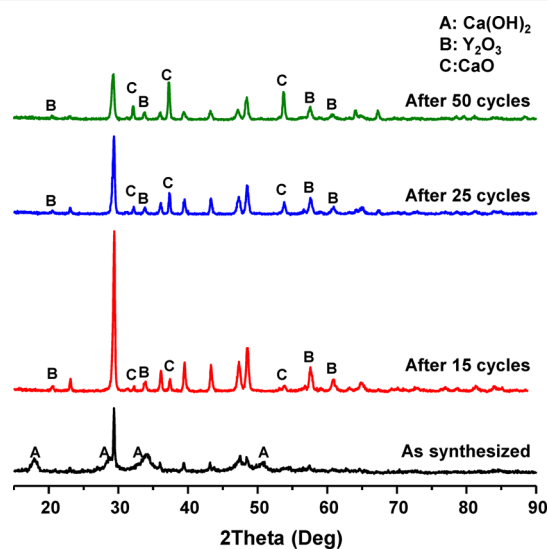

Figure 4. XRD patterns of the sample with 80:20 wt % CaO:Y_2O_3 synthesized at 700 °C. From bottom to top: after collection from the USP setup, after 15 cycles, after 25 cycles, and after 50 cycles of calcination/carbonation. The XRD patterns of $CaCO_3$, $Ca(OH)_2$, CaO, and Y_2O_3 are from ICDD PDF Fiel Card Nos. 04-007-8659, 00-001-1079, 04-005-4757, and 01-079-1257, respectively. Unlabeled peaks correspond to $CaCO_3$.

Figure 5. XRD patterns of the sample with 80:20 wt % CaO:$Ca_{12}Al_{14}O_{33}$. From bottom to top panel: after collection from the USP setup, after 15 cycles, after 25 cycles, and after 50 cycles of calcination/carbonation. The XRD patterns of $CaCO_3$, $Ca_{12}Al_{14}O_{33}$, $Ca_3Al_2O_6$, and CaO are from ICDD PDF File Card Nos. 04-007-8659, 00-009-0413, 04-008-8069, and 04-005-4757, respectively. Unlabeled peaks correspond to $CaCO_3$.

CaO:Y_2O_3 and CaO:$Ca_{12}Al_{14}O_{33}$, respectively. Formation of mixed oxide phases such as $Ca_{12}Al_{14}O_{33}$ and $Ca_3Al_2O_6$ in the case of aluminum-containing sample is considered to be effective in impeding sorbent sintering, when compared to the yttrium-containing sample. As sorbents go through cycling, peaks of unreacted CaO after carbonation are evident,
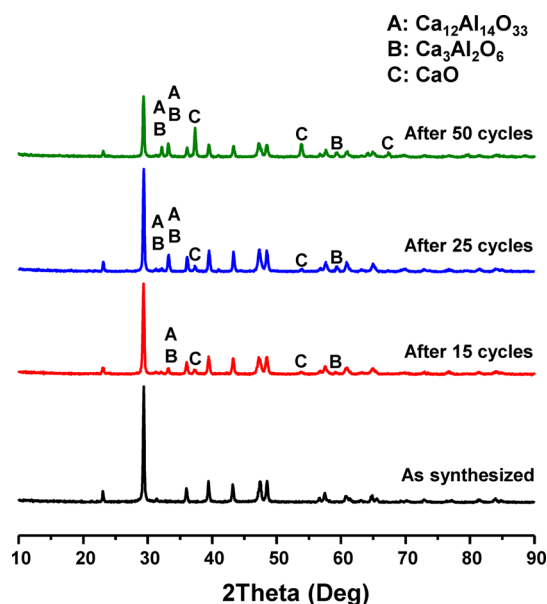
indicating the partial deactivation of sorbents (presumably in regions not readily accessible to CO_2 permeation and reaction, i.e., pore closure[21]). Longer term exposure to CO_2 permits regeneration of the sorbent; Figure S4 in the Supporting Information shows an increase in CO_2 capacity of Al/Ca composite sorbent when the adsorption time increased to 3 h. This suggests that sintering and pore closure over many cycles has affected CO_2 diffusion rate to unreacted CaO and has made

CO_2 sorption into the core of the sorbent a mass-transfer-limited process.

To describe the gas−solid carbonation reaction between carbon dioxide and composite CaO-based sorbents at elevated temperatures, a variable diffusivity shrinking core model with expanding product layer was adopted.[22] The model is an extension of the classical shrinking core model[23,24] and assumes three steps for the reaction, namely (1) the diffusion of gaseous reactant through the gas film around the particle to reach to the surface of the solid, (2) diffusion of gaseous reactant through the porous product layer to the surface of unreacted sorbent, and (3) eventual surface reaction of gaseous reactant at the surface of the unreacted sorbent (as illustrated in Figure S5 in the Supporting Information).

Three further assumptions are made. Because of a pure CO_2 gas stream used during the TGA runs, the mass-transfer resistance of the gas film surrounding the particle does not exist. In addition, the radius of the spherical particles increases as the reaction proceeds due to the difference between the molar volumes of the solid reactant (e.g., CaO) and the product (e.g., $CaCO_3$). And, finally, the diffusivity of gaseous reactant through the product layer is allowed to vary; the strong dependency of product layer diffusivity on the temperature, concentration, conversion, and depth in the product layer has been reported previously for the similar gas−solid reactions.[25−29]

Based on the above assumptions, the rate of change in the conversion (X) is given by

$$\frac{dX}{dt} = -\frac{\frac{3}{r_p}\frac{k_s}{N_{CaO}^0}(C_b - C_e)(1 - X)^{2/3}}{1 + \frac{k_s}{D_e}r_p(1 - X)^{1/3}\left(1 - \sqrt[3]{\frac{1 - X}{1 - X + XZ}}\right)} \qquad (1)$$

where C_b is the CO_2 concentration in the bulk gas, C_e is the equilibrium CO_2 concentration, D_e is the effective product layer diffusivity of CO_2, r_p is the initial radius of the particle, and N_{CaO}^0 is the initial number of moles of CaO per unit volume. Z is the expansion factor of the particle, defined as the ratio of the total volume of the reacted particle to the total volume of the unreacted particle and was assumed a constant value for all the composite sorbents. Table S1 in the Supporting Information lists the values for aforementioned parameters in the equation above. k_s is the surface reaction rate constant for each sample calculated from the initial slope of the first cycle conversion curve obtained from TGA data. The surface reaction rate constant for each composite sorbent is reported in Table 2. The k_s values obtained for different sorbents are not significantly different, which is as expected, given that the particle size and surface area of the fresh sorbents made by USP are all similar.

In this model, the dependence of the effective diffusivity through the porous product layer, with respect to conversion,

Table 2. Values of Surface Reaction Constant for Composite CaO-Based Sorbents

sorbent	Surface Reaction Constant, k_s ($\times 10^5$ m/s)
Y/Ca	1.34
Mg/Ca	1.41
Al/Ca	1.54
Si/Ca	1.63
Si/Al/Ca	1.43
pure CaO	1.63

was assumed to decay according to the following exponential function:

$$D_e = D_e^0 \exp(-\alpha X^\beta) \qquad (2)$$

where D_e^0 is the initial effective diffusivity, and α and β are two model parameters. The linear ordinary differential equation (ODE), along with the governing equation of the variable diffusivity shrinking core model, were solved and the model parameters (α and D_e^0) were determined using a multivariable regression method. In all cases, a value of $\beta = 3$ provided the least-squares of the errors fitting the TGA experimental data.

A representative comparison of the model predictions with the experimental TGA data in the cyclic process for the 80:20 wt % $CaO:Ca_2SiO_4$ composite sample is presented in Figure 6.
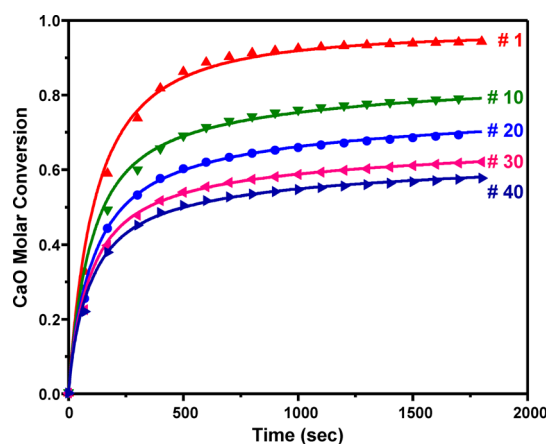

Figure 6. Comparison of the model predictions with the experimental TGA data in the cyclic process for the 80:20 wt % $CaO:Ca_2SiO_4$ composite sample. Points on the graphs represent the experimental data regarding carbonation for the shown cycles under 100% CO_2 at 700 °C, and solid lines represent the model predictions.

The model provides an excellent fit to the experimental data with $R^2 = 0.99$. The accuracy and qualitative behavior of the model predictions for all the other samples are very similar to this case and overall are in excellent agreement with the data presented in Figure 1.

The decrease in CO_2 capacity of CaO-based sorbents in a multicycle operation is mainly attributed to a decrease in surface area and a loss of porosity caused by sorbent sintering,[7,30−32] which is consistent with our observation in Figures 2c and 3c. These effects translate into a lower initial effective diffusivity that represents a less-permeable porous product layer for the gaseous reactant diffusion as the number of carbonation/regeneration cycles increases and also a higher tendency to pore closure at high conversions in each cycle. This is illustrated in Figure 7 for an example case of pure CaO sample. The drop in effective diffusivity with increase in CaO carbonation due to pore closure has also been reported in the sulfidation of a dolomite-based sorbent[33] and in the CaO carbonation process.[21]

In addition, the degree of enhancement in the cycling stability of the synthesized CaO-based sorbents can be quantified from the fitted model parameters, initial effective diffusivity (D_e^0) and diffusivity decay ratio (α). As illustrated in Figure 8a and Figure 8b, D_e^0 and α of pure CaO sample are compared to those of the doped materials through the cycling process. The presence of the metal oxide binders leads to a
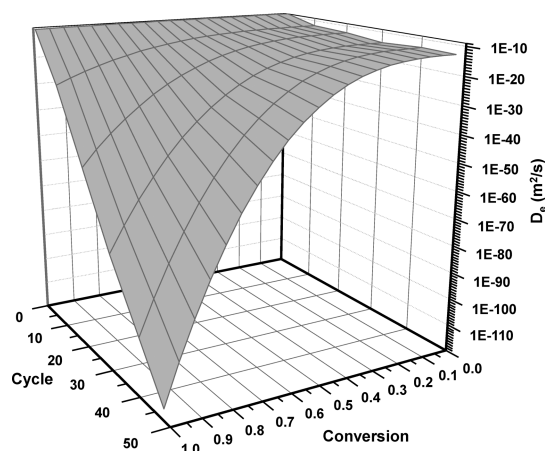
Figure 7. Decrease in the calculated effective diffusivity (D_e) for the pure CaO sample due to sintering during cycling process and also in each cycle with increase in CaO carbonation due to pore closure.

significant improvement in CO_2 diffusion through $CaCO_3$ product layer, as evidenced by a greater D_e^0 value, compared to the pure CaO sample (Figure 8a). Comparing the diffusivity decay ratio (α) values in Figure 8b further supports the enhancing effect of dopants in maintaining the stability of the sorbents over an increased number of cycles. The smallest calculated values of α and the largest calculated values of D_e^0 belong to the Si/Al/Ca sample, which was shown to retain the highest CO_2 capacity during 50 cycles among all the materials tested (Figure 1).

Two sets of power-law and second-order polynomial trend lines were used to fit the variations of D_e^0 and α during cycling in Figure 8a and Figure 8b, respectively. It is worth noting that the D_e^0 and α data for the first 10 cycles were not considered for curve fitting and extrapolation in order to eliminate the effect of the sorbent's activation/conditioning during the initial cycles. In the first few cycles, the structure of sorbents is still under activation/conditioning process (as evidenced from XRD characterization), and it can take up to 20 cycles, depending on the crystalline structure of sorbents, to form a stable pore structure with an established behavior under cycling.[34]
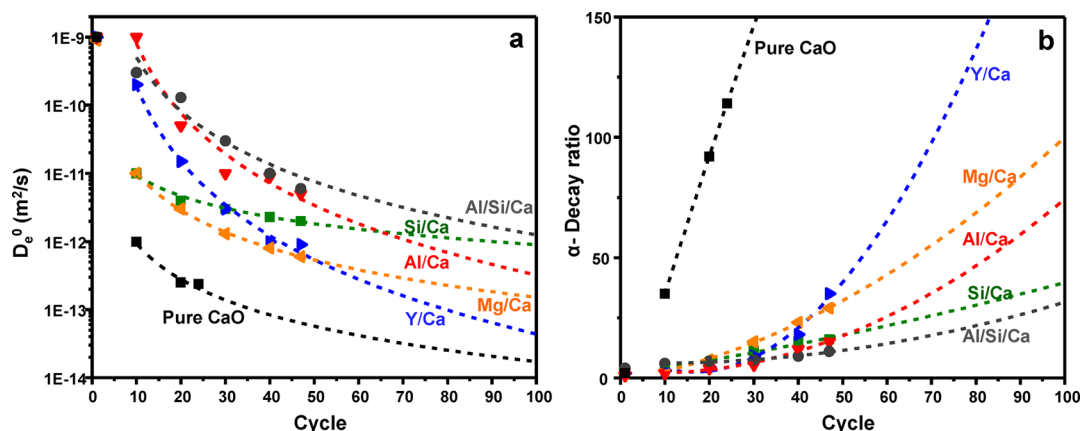
The trend lines are useful in extrapolation of the sorbent's performance and estimation of the fresh sorbent makeup rate in a continuous regenerative CO_2 capture process involving an increased number of cycles. As an example, the extrapolated values of D_e^0 and α were used to model a TGA run for a Al/Ca sample that had undergone 95 carbonation/regeneration cycles. Figure 9 compares the predicted CaO conversion, based on the
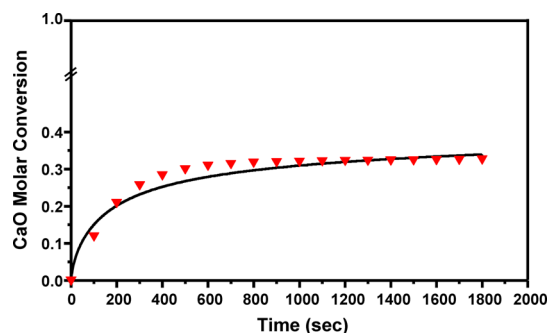

Figure 9. Comparison of the model prediction with the experimental TGA data of the Al/Ca composite sample at the 95th cycle. Points represent the experimental TGA data, while the solid line is the model prediction based on the extrapolated D_e^0 and α values at the 95th cycle.

extrapolated D_e^0 and α value with the experimental data obtained by TGA for the 95th cycle. The result reveals that the extrapolation gives an excellent prediction of performance of this sample after 95 carbonation/regeneration cycles with $R^2 = 0.97$. Thus, the same method could be used for extrapolation of the performance of other sorbents.

4. CONCLUSIONS

We have synthesized and characterized a series of composite CaO-based sorbents prepared by ultrasonic spray pyrolysis. Several refractory metal oxides with high melting temperatures were incorporated into a CaO matrix to enhance the reversibility of CaO in cyclic operation. The effect of added refractory oxides was compared, using sorbents with an 80 wt % CaO content. Among all the materials tested, the composite Si/Al/Ca sorbent with 80:10:10 wt % $CaO:Ca_{12}Al_{14}O_{33}:Ca_2SiO_4$ retained the highest CO_2 capacity after 50 carbonation/

Figure 8. (a) Calculated initial product layer diffusivity (D_e^0), and (b) diffusivity decay ratio (α) for composite CaO-based sorbents compared with pure CaO over 50 cycles. Two sets of power-law and second-order polynomial trend lines predict the sorbent's performance in an increased number of cycles. Al/Si/Ca sorbent possesses the highest product layer diffusivity and the smallest diffusivity decay ratio, which is consistent with its highest performance observed in Figure 1.

regeneration cycles. Furthermore, a variable diffusivity shrinking core model with expanding product layer was adopted to describe the gas–solid carbonation reaction involving carbon dioxide and the composite CaO-based sorbents. The model is able to predict the experimentally observed improved stability of the sorbents under cycling. The model provides an explanation for the effect of sintering and agglomeration on the performance of the sorbent through an introduction of a variable effective diffusivity. The model, as demonstrated, could also be used as a powerful tool to accurately extrapolate sorbent performance at a significantly high number of cycles.

ASSOCIATED CONTENT

Ⓢ Supporting Information

Supporting Information includes a schematic of the ultrasonic spray pyrolysis (USP) setup and additional material characterization. The Supporting Information is available free of charge on the ACS Publications website at DOI: 10.1021/acs.energyfuels.5b00397.

AUTHOR INFORMATION

Corresponding Author
*Tel.: 217-333-2794. Fax: 217-244-3186. E-mail: ksuslick@illinois.edu.

Author Contributions
The manuscript was written through contributions of all authors. All authors have given approval to the final version of the manuscript.

Notes
The authors declare no competing financial interest.

ACKNOWLEDGMENTS

REFERENCES

(1) Eide, L. I.; Bailey, D. W. *Oil Gas Sci. Technol.* **2005**, *60*, 475−484.
(2) Lee, K. B.; Beaver, M. G.; Caram, H. S.; Sircar, S. *Ind. Eng. Chem. Res.* **2008**, *47*, 8048−8062.
(3) Breault, R. W. *Energies* **2010**, *3*, 216−240.
(4) Barker, R. *J. Appl. Chem. Biotechnol.* **1973**, *23*, 733−742.
(5) Barker, R. *J. Appl. Chem. Biotechnol.* **1974**, *24*, 221−227.
(6) Abanades, J. C. *Chem. Eng. J.* **2002**, *90*, 303−306.
(7) Abanades, J. C.; Alvarez, D. *Energy Fuels* **2003**, *17*, 308−315.
(8) Valverde, J. M. *J. Mater. Chem. A* **2013**, *1*, 447−468.
(9) Bang, J. H.; Suslick, K. S. *Adv. Mater.* **2010**, *22*, 1039−1059.
(10) Messing, G. L.; Zhang, S.-C.; Jayanthi, G. V. *J. Am. Ceram. Soc.* **1993**, *76*, 2707−2726.
(11) Sayyah, M.; Ito, B. R.; Lu, Y.; Rostam-Abadi, M.; Suslick, K. S. *RSC Adv.* **2013**, *3*, 19872−19875.
(12) Li, Z.-s.; Cai, N.-s.; Huang, Y.-y. *Ind. Eng. Chem. Res.* **2006**, *45*, 1911−1917.
(13) Derevschikov, V. S.; Lysikov, A. I.; Okunev, A. G. *Ind. Eng. Chem. Res.* **2011**, *50*, 12741−12749.
(14) Liu, W.; Feng, B.; Wu, Y.; Wang, G.; Barry, J.; Diniz da Costa, J. C. *Environ. Sci. Technol.* **2010**, *44*, 3093−3097.
(15) Li, Y.; Zhao, C.; Ren, Q.; Duan, L.; Chen, H.; Chen, X. *Fuel Process. Technol.* **2009**, *90*, 825−834.
(16) Hlavac, J. *Pure Appl. Chem.* **1982**, 681−688.
(17) Wang, M.; Lee, C.-G.; Ryu, C.-K. *Int. J. Hydrogen Energy* **2008**, *33*, 6368−6372.
(18) Valverde, J. M.; Perejon, A.; Perez-Maqueda, L. A. *Environ. Sci. Technol.* **2012**, *46*, 6401−6408.
(19) Han, C.; Harrison, D. P. *Chem. Eng. Sci.* **1994**, *49*, 5875−5883.
(20) Chen, H.; Zhao, C.; Ren, Q. *J. Environ. Manage.* **2012**, *93*, 235−244.
(21) Mess, D.; Sarofim, A. F.; Longwell, J. P. *Energy Fuels* **1999**, *13*, 999−1005.
(22) Abbasi, E.; Hassanzadeh, A.; Abbasian, J. *Fuel* **2013**, *105*, 128−134.
(23) Levenspiel, O. *Chemical Reaction Engineering*, 3rd Edition; John Wiley & Sons: New York, 1999.
(24) Yagi, S.; Kunii, D. In *5th Symposium (International) on Combustion*; Proceedings of the Combustion Institute, Vol. 5; Elsevier: Amsterdam, 1955; p 231.
(25) Haul, R.; Stein, L. H. *Trans. Faraday Soc.* **1955**, *51*, 1280−1290.
(26) Anderson, T. F. *J. Geophys. Res.* **1969**, *74*, 3918−3932.
(27) Krishnan, S. V.; Sotirchos, S. V. *Can. J. Chem. Eng.* **1993**, *71*, 734−745.
(28) Stendardo, S.; Foscolo, P. U. *Chem. Eng. Sci.* **2009**, *64*, 2343−2352.
(29) Szekely, J.; Evans, J. W. *Metall. Trans.* **1971**, *2*, 1691−1698.
(30) Sun, P.; Grace, J. R.; Lim, C. J.; Anthony, E. J. *Ind. Eng. Chem. Res.* **2008**, *47*, 2024−2032.
(31) Wu, Y.; Blamey, J.; Anthony, E. J.; Fennell, P. S. *Energy Fuels* **2010**, *24*, 2768−2776.
(32) Grasa, G. S.; Abanades, J. C. *Ind. Eng. Chem. Res.* **2006**, *45*, 8846−8851.
(33) Adánez, J.; García-Labiano, F.; Abad, A.; de Diego, L. F.; Gayán, P. *Energy Fuels* **2000**, *15*, 85−94.
(34) Gasvaskar, V. S.; Abbasian, J. *Ind. Eng. Chem. Res.* **2011**, *51*, 213−217.